J. Micromech. Microeng. **17** (2007) 2077–2083 doi:10.1088/0960-1317/17/10/020

A microfluidic chaotic mixer using ferrofluid

Dong-Wook Oh[1], Jae Sik Jin[1], Jai Hyun Choi[2], Ho-Young Kim[1] and Joon Sik Lee[1]

[1] School of Mechanical and Aerospace Engineering, Seoul National University, Seoul 151-744, Korea
[2] Digital Media Business, Samsung Electronics Co, Suwon, Gyeonggi-do 422-600, Korea

E-mail: jslee123@snu.ac.kr

Received 12 March 2007, in final form 8 June 2007
Published 7 September 2007
Online at stacks.iop.org/JMM/17/2077

Abstract
A novel micromixer which utilizes chaotic mixing induced by ferrofluid actuation is developed. The micromixer is fabricated by a polydimethylsiloxane micromolding technique. The micromixer consists of a T-shaped main mixing channel and two parallel sub-channels that intersect the main channel. Oscillation of a couple of ferrofluid slugs in the sub-channels, induced by external permanent magnet actuation, generates chaotic advection in the main channel flow. To visualize the mixing, red fluorescent particles are supplied to one of the inlets of a T-shaped channel, and mixing flow is observed by a fluorescence microscope and an intensified CCD camera. The mixing experiments are performed with various ferrofluid perturbation frequencies and main stream flow velocities. The optimal mixing conditions determining the upper and lower limits of the most effective Strouhal numbers are found from the experimental results.

1. Introduction

Controlling fluid motions and chemical reactions in microfluidic systems for bio-chemical application has been an area of great interest recently. Considerable advantages are conferred by miniaturization, such as smaller reagent volumes, shorter reaction times and parallel operations, so that it is possible to integrate an entire conventional laboratory onto a single chip [1–3].

Homogeneous mixing of fluid reagents is essential in such microfluidic systems. But mixing fluids on microscales is difficult due to inherently low Reynolds number (Re) of microchannel flows, generally less than 100. Here the Re is defined as $U_m D_h/\nu$, where U_m is the average main stream velocity, D_h is the hydraulic diameter of the microchannel and ν is the kinematic viscosity of the fluid. In this Re range, the mixing is dominated entirely by molecular diffusion where an extremely long mixing channel is needed. Thus, diffusion-dependent micromixers are hardly acceptable for design requirements for lab-on-a-chip (LOC) or micro-total analysis system (μ-TAS). To overcome this inefficient mixing performance dominated by diffusion, various mixers have been suggested to utilize chaotic advection.

Chaotic advection can be introduced to the microchannel flow in either passive or active ways [4–14]. Chaotic advection can be generated in passive mixers by three-dimensional serpentine microchannels [4], by patterned grooves on the channel floors [5] and in droplets moving through a winding channel [6]. Active mixers employ a stirring effect by a rotating magnetic bar [7], oscillatory flow generated by thermal bubble actuation [8], ultrasonic vibration on continuous flow [9], electrokinetic flow driven by a channel wall's electric potential variation [10] and periodic pressure perturbation in cross-channels [11].

Active mixers have great advantages in mixing rate and its control. Although the lack of moving parts makes passive mixers free of additional friction and wear effects, their intricate channel topologies are often hard to microfabricate, and they are generally not switchable. On the other hand, active mixers are suitable, due to their controllability, for the reconfigurable microfluidic systems in which various functions are performed through external control inputs [12]. Among the active mixers, a mixer driven by external magnetic force, with magnetic particles or microneedles immersed in the fluid, has benefits in its simple design fabrication process [13].

In this study, magnetically actuated ferrofluid plugs are utilized to generate perpendicular periodic pressure oscillation in the main stream. With soft lithography fabrication of polydimethylsiloxane (PDMS) microchannels, ferrofluid actuation can be integrated with low cost, disposable microfluidic systems including micropumps and valves [14, 15]. A ferrofluid micromixer designed in this work has precise and flexible control of perturbation frequency. This enables the quantification of the fluid mixing rate for various perturbation frequencies. Thus, optimal oscillation frequency can be determined for required mixing rate in LOC or μ-TAS, where a volume flow rate is typically given as a key design parameter. In section 2, we describe the chaotic mixing and the ferrofluid mixer. Then microchannel fabrication and experimental setup are explained in section 3. In section 4, experimental observations are presented, and finally a summary and conclusion are given in section 5.

2. Chaotic mixing and the ferrofluid mixer

To enhance the mixing of two heterogeneous fluids, maximization of the interfacial area through external perturbation is essential. The mixing performance depends on the efficiency of stretching and folding of the interfacial area. When the flow field is externally perturbed, the fluid lump is stretched and folded by the chaotic advection. A measure of the mechanical mixing state is given by the average thickness of the two fluid layers, the striation thickness. It is well known that the ratio between the striation thickness and the channel hydraulic diameter decreases exponentially as the mixing fluids are exposed in the chaotic advection environment [16].

The mixing phenomenon in the cross-channel mixer is characterized as chaotic mixing, according to the study of Niu and Lee [17], and the mixing performance is related to the perturbation amplitude and frequency. At the cross-channel junctions, the interfacial line that separates the to-be-mixed fluids is stretched and folded by transversal perturbation. The stretching and folding is augmented by streamwise velocity gradient in the perturbation flow stream. The stretched and folded interfacial line is shown in figure 1, in the absence of the main stream velocity. Further stretching and folding takes place when perturbation flow meets the main stream flow. Not only the parabolic profile of main stream velocity comes into play, but also additional distortion of the interfacial line is induced by the four corners A, B, C and D in the cross-channel junctions as shown in figure 1. In this study, a chaotic mixer with two cross-channel junctions is considered.

The T-shaped main stream channel with two perpendicular actuation channels is fabricated as depicted in figure 2(*a*). The image of the sub-channel with ferrofluid plugs is also shown in the inset of figure 2(*a*). The designed height of the overall microchannel is 100 μm whereas the widths of main stream and of the perturbation channel are both 200 μm. The two cross-channel junctions are 200 μm apart. Figure 2(*b*) shows a schematic of the mixing region and the two parallel sub-channels with a ferrofluid plug. Transversal pressure oscillation caused by the ferrofluid displacement is imposed on the main stream flow. The ferrofluid plugs are actuated by an external permanent magnet and a linkage system, and

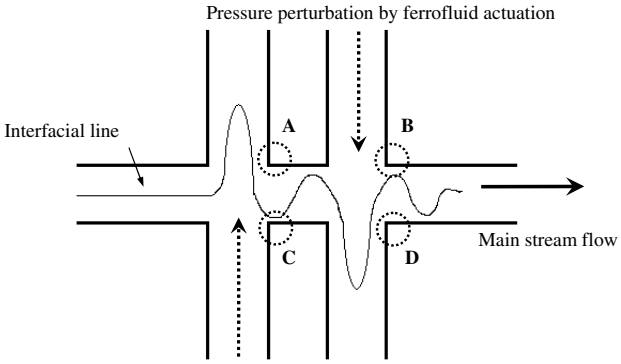

Figure 1. Perturbing perpendicular flow in the two junctions of a cross-channel mixer. At the four corners, A, B, C and D, additional distortion of the interfacial line is induced.

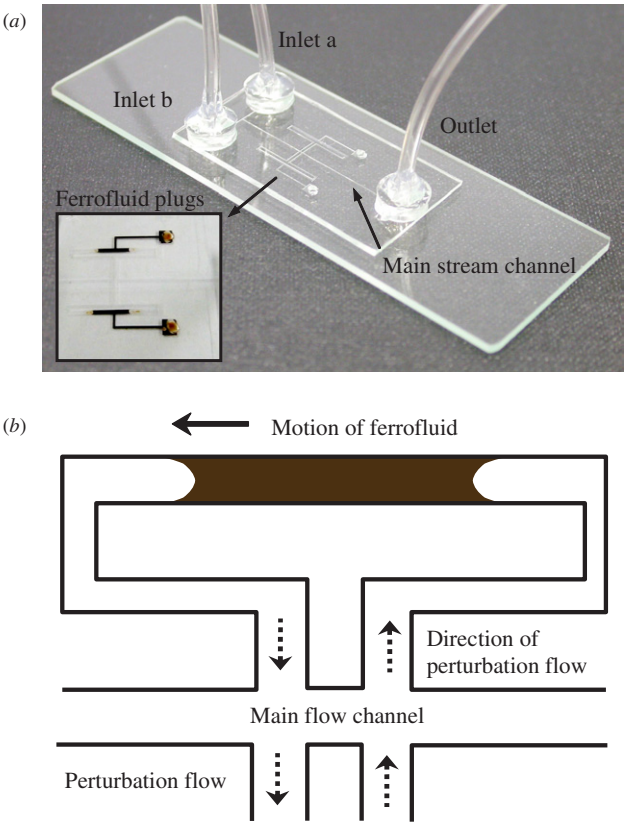

Figure 2. Ferrofluid actuated cross-channel micromixer. (*a*) Picture of a micromixer with an image of the ferrofluid plug in the inset. (*b*) Schematic of half a cycle ferrofluid actuation mechanism showing the motion of the ferrofluid plug and the corresponding direction of perturbation flows to the main flow channel.

this will be discussed in section 3.3 with details. With half a cycle of ferrofluid movement, crossing transversal flow at two cross sections is generated as shown in figures 1 and 2(*b*). In the next half cycle, the direction of the crossing transversal flow is reversed. This mechanism is expected to enhance the mixing performance significantly compared to the single cross-channel mixers as the lamination of the flow is further reoriented by multiple side channels [17]. Furthermore, the width of the channel in which ferrofluid plugs are situated is set as 400 μm, twice as wide as the perturbation channel, to emphasize the pressure oscillation effect on the main stream

flow. With this actuating system, we cannot only control the ferrofluid movement with great ease and accuracy, but various frequencies of perturbation can also be imposed on the main stream flow with a constant amplitude.

The PDMS soft lithography technique is selected as the microchannel fabrication method because of its cost advantage, ease of fabrication and applicability to the disposable microfluidic systems. The fabrication process of the micromixer is described in the following section.

3. Microchannel fabrication and experimental setup

3.1. Microchannel fabrication

The 100 mm diameter silicon wafer which is used as the mold substrate for PDMS microchannel replica is initially cleaned in a piranha solution for 10 min. The negative photoresist SU-8 is spin-coated on the silicon wafer with a thickness of 100 μm. Then the SU-8 coated silicon wafer is placed on a leveled plate and left overnight. During this waiting time, the uniformity in thickness is greatly enhanced by freeing bubbles that are confined in the SU-8 layer of a viscous liquid state and by flattening the edge bead. After softbaking the SU-8 coated wafer at 95 °C on a hotplate for 20 min, UV exposure is done with a mask aligner. Post-exposure bake is carried out at 95 °C with slow (2 °C min^{-1}) temperature ramping and cooling to prevent thermal cracks within the SU-8 layer which are commonly observed when it is rapidly heated and cooled. Slow temperature ramping and cooling is also required to enhance SU-8 adhesion to the silicon wafer. The wafer is developed with an SU-8 developer for 10 min and rinsed in isopropyl alcohol (IPA), then dried in open air for 10 min.

PDMS is prepared by mixing the Sylgard 184 base and curing agent, purchased from Dow Corning, in a 10:1 weight ratio. The mixture of base and curing agent is put inside the vacuum chamber until the bubbles inside the liquid-state PDMS are not visible. The volume of PDMS poured onto the silicon wafer mold is controlled so that the thickness of each PDMS replica is approximately 0.6 mm. Thin PDMS layers are preferred for effective magnet actuation of ferrofluid plugs, in general. The cured PDMS is then peeled off from the silicon wafer mold and cut into appropriate sizes to be bonded to the cover glass. The holes for inlet, outlet and ferrofluid injection reservoirs on the PDMS replica are punched before bonding to the cover glass. The PDMS replica is cleaned in acetone and IPA prior to O_2 plasma surface treatment for glass–PDMS bonding. The surface of PDMS is treated with oxygen plasma in a reactive ion etching (RIE) system. The replica is then bonded to a cover glass. Donut shaped cylinder PDMS blocks are additionally prepared and bonded on inlets and outlet of the already bonded micromixer and cover glass assembly for tubing. Finally, silicone tubes are inserted into the cylinder blocks and sealed with silicone rubber to prevent any leakage.

3.2. Optical imaging system

De-ionized (DI) water is used as the working fluid. At the inlet a, in figure 2, DI water containing fluorescent polymer particles (Duke Scientific Corp.) is supplied, while pure DI water is supplied at the inlet b. The fluorescent particles used in our experiments have a Stokes shift of 70 nm, excitation and emission maxima wavelengths of 542 nm and 612 nm, respectively.

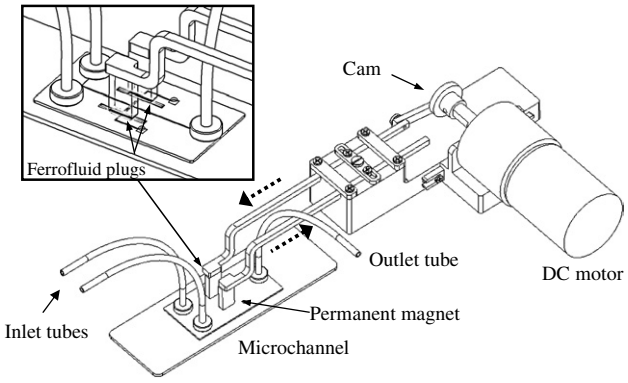

Figure 3. Schematic of permanent magnet actuation system. The dotted arrows show the direction of the permanent magnet motion at half a cycle of dc motor revolution.

An epi-fluorescent inverted microscope (IX71, Olympus) is utilized to visualize the mixing performance in the microchannel. A mercury lamp is used as the light source and light of wavelength 510–550 nm is transmitted through the objective lens. The fluorescent particles seeded in the working fluid are excited by the filtered light source and emit longer wavelength light. A 590 nm high pass filter filters the emitted light from the fluorescent particles, and finally, flow images in the mixing channel are taken by an intensified CCD (ICCD) camera (DiCAM-PRO, The Cooke Corp.) connected to a computer.

3.3. Micromixer and actuating system assembly

Before the assembly of the micromixer and the external actuation system, the fabricated PDMS microchannel is filled with DI water and put in the vacuum chamber where the pressure is maintained below 10 Pa for 1 min. By repeating this process a couple of times, most air bubbles contained within the water-filled microchannel could be removed. The ferrofluid (ACP E18, Ferrotec Corp.) immiscible with water is then injected through the punched hole into the ferrofluid reservoir indicated in the inset of figure 2(*a*). The amount of ferrofluid injection is carefully controlled so that the length of the ferrofluid plug inside the actuation channel is 5 mm. The ferrofluid injection hole is then sealed with cellophane tape to prevent leakage of the ferrofluid and water.

The microchannel is put on the microscope stage and a permanent magnet actuation system is placed on top of the PDMS layer. The permanent magnet is fixed to a linkage that converts rotational motion of the dc motor to reciprocal transversal movement. A schematic of the assembled PDMS microchannel and the permanent magnet actuation system is shown in figure 3. The dc motor and the linkage assembly are set up on a stage that can control the permanent magnet elevation with micrometer resolution. The permanent magnet is brought down as close to the ferrofluid plugs as possible to maximize the magnetic actuation performance. The stage is put on a vibration isolation rubber layer to minimize the fluid flow disturbance.

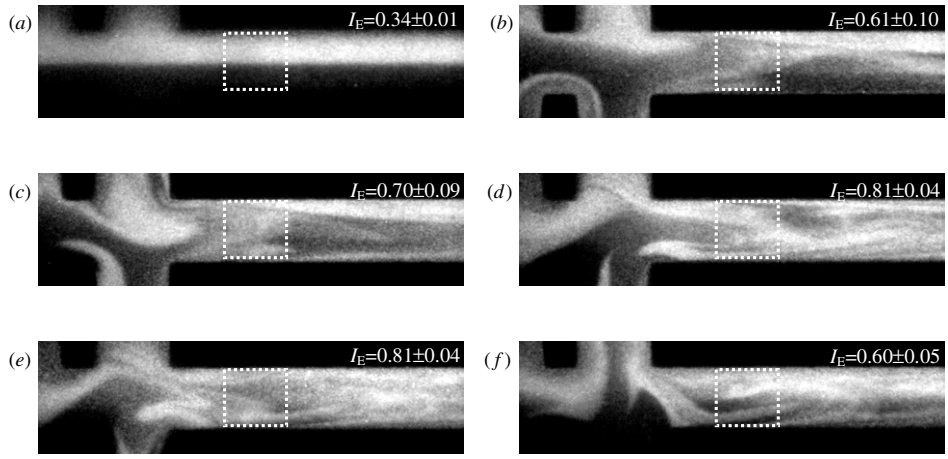

Figure 4. Fluorescent microscopy image downstream of cross channel with various perturbation frequencies at $Re = 0.35$. (*a*) 0 Hz, (*b*) 2 Hz, (*c*) 4 Hz, (*d*) 6 Hz, (*e*) 8 Hz and (*f*) 10 Hz.

The transversal distance that the permanent magnets travel during a single dc motor revolution is fixed to 5 mm, by the size of the cam. The dotted arrows in figure 3 show the directions of the permanent magnet motion at half a cycle of dc motor revolution. The corresponding displacement of the ferrofluid plug is observed to be approximately 0.5 mm throughout the whole actuation frequency range. This is due to the wetting nature of the ferrofluid to the PDMS walls which works as resistance to the ferrofluid plug movement within the microchannel.

The maximum frequency response limit of ferrofluid can be estimated by comparing the orders of the inertial force of the moving ferrofluid/water plug and the attractive magnetic force of the permanent magnet. The inertial force (F_i) of a moving ferrofluid can be written as $F_i = mwf^2$, where m is the mass of the moving fluid plug, w is the plug movement length, and f denotes the perturbation frequency. The actuation force can be approximated by attractive magnetic force exerted on the ferrofluid plug. Although this is a crude approximation, it is acceptable for an order of magnitude comparison of two forces. The attractive magnetic force (F_a) of two parallel plates with a negligible distance can be written as $F_a = AB^2/2\mu$, where A denotes the area of parallel plates, B is the surface magnetic field of the plates, and μ is the magnetic permeability. In our case, the cross-sectional area of the ferrofluid plug, the surface magnetic field of the permanent magnet given by the manufacturer and the magnetic permeability of water can be used to calculate the attractive magnetic force exerted on the ferrofluid. The above two forces are calculated by using the following parameters: $m = 4 \times 10^{-4}$ g, $w = 0.5$ mm, $A = 4 \times 10^{-8}$ m^2, $B = 50$ mT and $\mu = 1.26 \times 10^{-6}$ T m A^{-1}. In order for the inertial force and the magnetic force to be comparable, f needs to be of the order of 450 Hz. Thus we may conclude that the frequency response limit of the ferrofluid is well beyond the highest perturbation frequency, 14 Hz, used in our experiments.

3.4. Experimental conditions

To analyze the mixing behavior, various perturbation frequencies are delivered to the ferrofluid plug at different main stream flow rates. The voltage input to the dc motor is controlled so that the perturbation frequency ranges from 1.5 to 14 Hz with an increment of 0.6 Hz.

Pressure-driven main stream flow is generated by a homemade syringe pump. An ac motor and various speed reduction gearbox combinations are used to control flow rates. The steady state of the main stream flow is achieved within 10 min after the ac motor is turned on. The flow rate is controlled from 1.9 to 4.7 μl min^{-1}. The corresponding Re varies from 0.17 to 0.52. The image of the microchannel cross section is taken by the ICCD camera at 8 frames s^{-1} and saved on the computer by the 8 bit gray scale bitmap file. One hundred images are taken for each set of flow velocity and perturbation frequency.

4. Experimental observations

4.1. Quantification of mixing rate

The observation of the fluorescence intensity along the microchannel cross section is used as the criterion of mixing. Figure 4 shows the cross-channel mixer images taken by the ICCD camera when the Re of main flow is maintained at 0.35. A flow which contains the fluorescent particles, shown as the bright area, can be clearly distinguished from the dark pure DI water flow. In addition, it is confirmed that mixing through mere molecular diffusion is negligibly weak since the separation of bright and dark areas is maintained throughout the downstream of the main channel as in figure 4(*a*) where no perturbation is given to the main flow. Calculation of the Peclet number (Pe), which is defined as the ratio between the rate of advection of the flow to that of the diffusion, can also verify the absence of molecular diffusion of the fluorescent particles. At the lowest main stream velocity, the Pe is calculated to be over 1.1×10^5, indicating that the mixing inside the micromixer is purely advection dominant. As the perturbation is imposed, the two layers of fluids are mixed and as a result, the bright area is widened downstream (figures 4(*b*)–(*f*)).

In this study, the mixing rate at different ferrofluid actuation frequencies is quantified by introducing a mixing index. The mixing index is obtained at a specific region

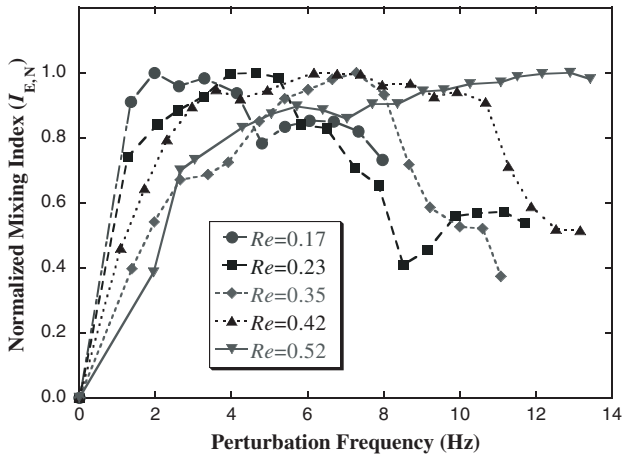

Figure 5. The normalized mixing index variation with respect to perturbation frequency and *Re*.

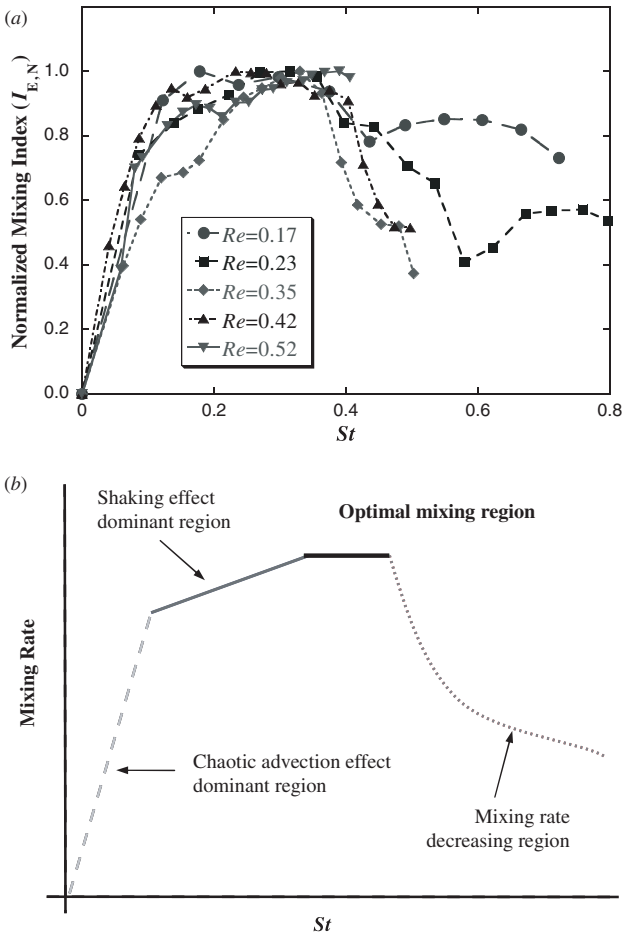

Figure 6. The behavior of the normalized mixing index with varying *St*. (*a*) Relationship between the normalized mixing index and the *St* at different *Re*. (*b*) A simplified schematic of the mixing rate profile versus *St*.

downstream of the cross channel. The region is selected as a square area of 180 × 180 μm^2, 200 μm downstream of the second junction of the micromixer as shown as the dotted square in figures 4(*a*)–(*f*). The corresponding area of 130 × 130 pixels in an 8 bit gray scale image taken by the ICCD camera is analyzed.

The brightness value for a single pixel varying from 0 to 255 is read at the selected region and the mixing index I_E is calculated as follows [4]:

$$I_E = 1 - \frac{1}{\bar{I}}\sqrt{\frac{1}{N}\sum (I_i - \bar{I})^2} \tag{1}$$

where $\bar{I}$ is the averaged brightness of the calculated region which is defined as $\bar{I} = \sum I_i/N$, N denoting the total number of pixels in the region, and I_i is the value of brightness of a single pixel. The calculated mixing indices show little deviation during a single cycle of perturbation at a given constant perturbation frequency. For example, the standard deviation value is generally less than 0.05 for perturbation frequencies higher than 4 Hz. However, 100 mixing index values have been averaged for each set of velocity and the frequency condition for reliability. The calculated mixing index and the standard deviation value for each corresponding perturbation frequency are labeled in figure 4. Ideally, in the case of non-mixing, the mixing index I_E becomes 0. For the fully mixed state, the mixing index should be unity. Thus additional normalization of the mixing index is introduced as follows for the clear comparison of each main stream velocity case:

$$I_{E,N} = \frac{I_E - I_{E,min}}{I_{E,max} - I_{E,min}} \tag{2}$$

where $I_{E,N}$ is the normalized mixing index for a given main stream velocity and perturbation frequency condition, $I_{E,min}$ is the minimum mixing index calculated from the set of mixing index data of a single velocity and $I_{E,max}$ is the maximum mixing index value.

4.2. Experimental results

The calculated results of the normalized mixing index with respect to the perturbation frequency and the *Re* of main stream flow are plotted in figure 5. At low ferrofluid actuation frequencies, the mixing performance is improved because the chaotic advection is introduced to the main stream flow by the perpendicular perturbation. As the folding and stretching in the fluids are promoted, a rapid increase of the mixing index is observed which is believed to be caused by the exponential nature of the chaotic advection mixing enhancement [17]. This steep slope in the normalized mixing index profile is noticed in the perturbation frequency range of 0–2 Hz. For the main stream flow of $Re = 0.17$, the fully mixed state is already achieved in this perturbation frequency region. When the *Re* is over 0.23, as the perturbation frequency increases, the normalized mixing index gradually increases until it reaches the maximum. In this region, the rate of increase of the normalized mixing index is clearly decreased compared with that of the low-frequency region. Although the explanation of such a phenomenon calls for more theoretical study, we provide a simple physical reasoning for the observed trend. The increase in the perturbation frequency no longer augments the already-existing chaotic advection effect in the cross channel. Only the 'shaking effect' of the perturbation flow to the main stream flow is added to the normalized mixing index. The shaking effect on the main flow is expected to be weaker in the mixing enhancement compared with the

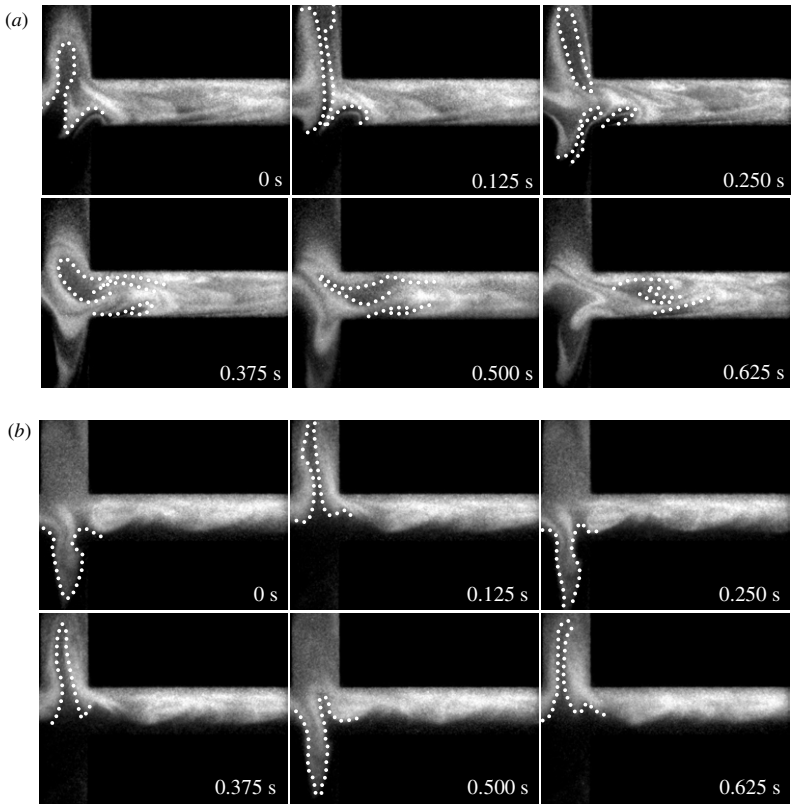

Figure 7. Sequential images of a fully mixed state and decreased mixing rate state at $Re = 0.35$. The interfacial lines separating the fluid regions with and without fluorescent particles are drawn as dotted lines. (*a*) $St = 0.36$, (*b*) $St = 0.50$.

exponential increase of the mixing rate that can be achieved via chaotic advection. By observing the downstream region in figures 4(*d*) and (*e*), nearly uniform distribution of fluorescent particles can be observed. However, further increase in the perturbation frequency results in a decrease in $I_{E,N}$ (figure 4(*f*)).

To simplify the dependence of the mixing efficiency on the perturbation frequency and the main stream flow rate, additional consideration is given to the relationship between the normalized mixing index and the Strouhal number (*St*). *St* can be defined as $f D_h / U_m$. The normalized mixing index versus the *St* is plotted as in figure 6(*a*). In figure 6(*a*), the scattered data in figure 5 tend to collapse into a single line and only a small discrepancy between each data set of different *Re* is observed. As can be seen in figure 6(*a*), the chaotic advection dominates the increase in the mixing rate when the *St* is smaller than 0.1. As *St* increases, the mixing rate gradually increases and reaches the maximum in the *St* range of 0.2–0.4. However, further increase of *St* exceeding 0.4 no longer increases the mixing rate. This indicates that at a high ferrofluid actuation frequency where the perturbation flow velocity overwhelms the velocity of the main stream flow, the mixing rate rather decreases. This agrees with the experimental result of Lee *et al* where the optimal mixing for a single cross-channel micromixer occurred at *St* close to 0.25 [18].

A further comparison is made for the *St* values of 0.36 and 0.5 at *Re* of 0.35. The sequential images of these conditions with the interfacial lines that separate the unmixed fluids are presented in figure 7. Under the fully mixed condition shown in figure 7(*a*), the interfacial region is stretched (0.125 s) by the perturbation flow until it ruptures (0.250 s). Additional folding of the isolated unmixed volume occurs (0.375 s) when the interfacial region passes the corners of the cross-channel junction and consequently the striation thickness decreases until it is not visible. In the case of figure 7(*b*), however, where an increase in the perturbation frequency obstructs the mixing, the fluctuating interfacial line is observed to be confined in the subchannel throughout the images. Such a mere oscillation of the interfacial line in the mixing region has also been observed in computational fluid dynamic simulation with Lagrangian flow analysis, in a cross-channel mixer [19] and pulsatile flow in a wavy channel [20]. This insufficient mixing behavior is somewhat analogous to the vibration isolation of a mass, spring and damper system where the mass is oscillated at a much higher frequency than the resonant frequency [21].

This behavior can be found under all velocity conditions tested, and the relationship between the mixing rate and the *St* within the cross-channel mixer can be schematically represented as in figure 6(*b*). The profile of the mixing rate variation can be classified into four regions of chaotic advection dominant, shaking effect dominant, fully mixed and mixing rate decreasing regions as the perturbation strength increases.

In order to define the fully mixed state quantitatively, we regarded the condition of $I_{E,N} \geqslant 0.95$ as the fully mixed state. The upper and lower *St* limits of the fully mixed state are plotted in figure 8 as functions of the average main stream velocity. The region enclosed by the two lines indicates the

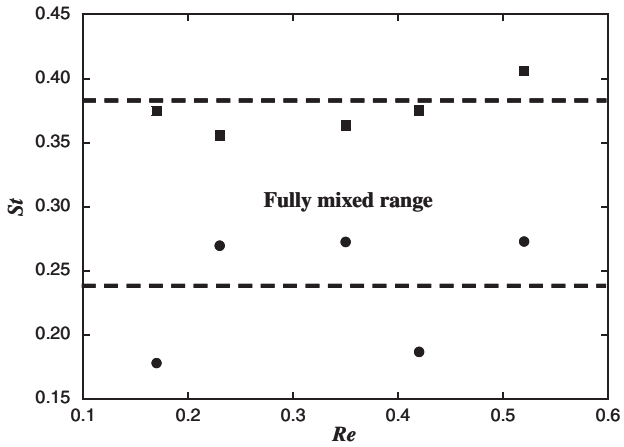

Figure 8. The relationship between *St* and *Re* to achieve a fully mixed region. The round and square marks indicate the lowest and the highest *St* to achieve a fully mixed condition at different *Re*. The dotted lines show the averaged low ($St = 0.24$) and high ($St = 0.38$) limits of *St* to achieve a fully mixed condition.

optimal region of the fully mixed state, and the average value of the upper and the lower limits of *St* are 0.24 and 0.38, respectively.

5. Conclusions

A micromixer using ferrofluid actuation is designed, and the experiments are conducted to observe the mixing performance in the microchannel with two cross-channel junctions. The ferrofluid micromixer developed in this work has such advantages as rapid mixing capability, low manufacturing cost and simple fabrication procedure.

The influence of perturbation frequency and main stream velocity on the mixing performance is quantified with the normalized mixing index, *St* and *Re*. It is experimentally found that the optimal region of *St* exists for efficient mixing. The mixing phenomenon inside the cross-channel mixer can be categorized depending on *St* into the following stages. When the *St* is smaller than 0.1, chaotic advection is dominant and the mixing is rapidly promoted with the perturbation frequency increase. While the *St* increases to around 0.2–0.4, the mixing rate is gradually increased and the optimal mixing state is achieved. However, further increase in the perturbation frequency or *St* results in a decrease in the mixing rate due to the vibration isolation effect.

Acknowledgments

The authors gratefully acknowledge financial support from the Micro Thermal System Research Center sponsored by the Korean Science and Engineering Foundation, Korea Research Foundation grant no. KRF-2004-R08-2004-000-10619-0.

References

[1] Beebe D J, Mensing G A and Walker G M 2002 Physics and applications of microfluidics in biology *Ann. Rev. Biomed. Eng.* **4** 261–86
[2] Figeys D and Pinto D 2000 Lab-on-a-chip: a revolution in biological and medical sciences *Anal. Chem.* **72A** 330–5
[3] Chován T and Guttman A 2002 Microfabricated devices in biotechnology and biochemical processing *Trends Biotechnol.* **20** 116–22
[4] Liu R H, Stremler M A, Sharp K V, Olsen M G, Santiago J G, Adrian R J, Aref H and Beebe D J 2000 Passive mixing in a three-dimensional serpentine microchannel *J. Microelectromech. Syst.* **9** 190–7
[5] Stroock A D, Dertinger S K W, Ajdari A, Mezic I, Stone H A and Whitesides G M 2002 Chaotic mixer for microchannels *Science* **295** 647–51
[6] Bringer M R, Gerdts C J, Song H, Tice J D and Ismagilov R F 2004 Microfluidic systems for chemical kinetics that rely on chaotic mixing in droplets *Phil. Trans. R. Soc. Lond.* A **362** 1087–104
[7] Lu L H, Ryu L S and Liu C 2002 A magnetic microstirrer and array for microfluidic mixing *J. Microelectromech. Syst.* **11** 462–9
[8] Tsai J H and Lin L 2002 Active microfluidic mixer and gas bubble filter driven by thermal bubble micropump *Sensors Actuators* **A 97–98** 665–71
[9] Yang Z, Matsumoto S, Goto H, Matsumoto M and Maeda R 2001 Ultrasonic micromixer for microfluidic systems *Sensors Actuators* A **93** 266–72
[10] Lee C Y, Lee G B, Fu L M, Lee K H and Yang R J 2004 Electrokinetically driven active micro-mixers utilizing zeta potential variation induced by field effect *J. Micromech. Microeng.* **14** 1390–8
[11] Dodge A, Jullien M C, Lee Y K, Niu X, Okkels F and Tabeling P 2004 An example of a chaotic micromixer: the cross-channel micromixer *C. R. Phys.* **5** 557–63
[12] Campbell C J and Grzybowski B A 2004 Microfluidic mixers: from microfabricated to self-assembling devices *Phil. Trans. R. Soc. Lond.* A **362** 1069–86
[13] Suzuki H and Ho C M 2002 A magnetic force driven chaotic micro-mixer *Proc. 15th Int. Conf. on Micro Electro Mechanical Systems (MEMS'02) (Las Vegas, NV)* pp 40–3
[14] Hartshorne H, Backhouse C J and Lee W E 2004 Ferrofluid-based microchip pump and valve *Sensors Actuators* B **99** 592–600
[15] Yamahata C, Chastellain M, Parashar V K, Petri A, Hofmann H and Gijs M A M 2005 Plastic micropump with ferrofluidic actuation *J. Microelectromech. Syst.* **14** 96–102
[16] Ottino J M 1989 *The Kinematics of Mixing, Stretching, Chaos and Transport* (New York: Cambridge University Press)
[17] Niu X and Lee Y K 2003 Efficient spatial–temporal chaotic mixing in microchannels *J. Micromech. Microeng.* **13** 454–62
[18] Lee Y K, Shih C, Tabeling P and Ho C M 2007 Experimental study and nonlinear dynamic analysis of time-periodic micro chaotic mixers *J. Fluid Mech.* **575** 425–48
[19] Okkels F and Tabeling P 2004 Spatiotemporal resonances in mixing of open viscous fluids *Phys. Rev. Lett.* **92** 038301
[20] Lee B S, Kang I S and Lim H C 1999 Chaotic mixing and mass transfer enhancement by pulsatile laminar flow in an axisymmetric wavy channel *Int. J. Heat Mass Transfer* **42** 2571–81
[21] Inman D J 2000 *Engineering Vibration* 2nd edn (Upper Saddle River, NJ: Prentice-Hall)